Current-Induced Magnetization Switching Behavior in Perpendicular Magnetized $L1_0$-MnAl/B2-CoGa Bilayer

Hong-Li Sun(孙宏利)[1,2], Rong-Kun Han(韩荣坤)[1,2], Hong-Rui Qin(秦红蕊)[1,2], Xu-Peng Zhao(赵旭鹏)[3], Zhi-Cheng Xie(谢志成)[1,2], Da-Hai Wei(魏大海)[1,2] and Jian-Hua Zhao(赵建华)[1,2*]

[1]*State Key Laboratory of Superlattices and Microstructures, Institute of Semiconductors, Chinese Academy of Sciences, Beijing 100083, China*
[2]*Center of Materials Science and Optoelectronics Engineering, University of Chinese Academy of Sciences, Beijing 100190, China*
[3]*International School of Microelectronics, Dongguan University of Technology, Dongguan 523808, China*

(Received 20 March 2024; accepted manuscript online 30 April 2024)

Rare-earth-free Mn-based binary alloy $L1_0$-MnAl with bulk perpendicular magnetic anisotropy (PMA) holds promise for high-performance magnetic random access memory (MRAM) devices driven by spin-orbit torque (SOT). However, the lattice-mismatch issue makes it challenging to place conventional spin current sources, such as heavy metals, between $L1_0$-MnAl layers and substrates. In this work, we propose a solution by using the B2-CoGa alloy as the spin current source. The lattice-matching enables high-quality epitaxial growth of 2-nm-thick $L1_0$-MnAl on B2-CoGa, and the $L1_0$-MnAl exhibits a large PMA constant of 1.04×10^6 J/m^3. Subsequently, the considerable spin Hall effect in B2-CoGa enables the achievement of SOT-induced deterministic magnetization switching. Moreover, we quantitatively determine the SOT efficiency in the bilayer. Furthermore, we design an $L1_0$-MnAl/B2-CoGa/Co_2MnGa structure to achieve field-free magnetic switching. Our results provide valuable insights for achieving high-performance SOT-MRAM devices based on $L1_0$-MnAl alloy.

DOI: 10.1088/0256-307X/41/5/057503

Magnetic random-access memory (MRAM) represents a promising avenue for next-generation storage devices within the semiconductor industry.[1,2] In MRAM technologies, modulating local magnetization via electrical methods is essential. Compared to two-terminal spin-transfer torque (STT) MRAM,[3,4] the spin-orbit torque (SOT) MRAM, as a three-terminal device, avoids the passage of large currents through the barrier of magnetic tunnel junction (MTJ), significantly enhancing the reliability and endurance of the device.[5–7] In the typical spin current generator (SCG)/ferromagnet (FM) bilayer, the SOT effect originates from the spin Hall effect (SHE) and interfacial Rashba–Edelstein effect.[8–10] For SHE, when applying a current along the x direction, y-polarized spins are separated in the z direction, accumulating at the interface and further influencing the adjacent FM layer. In films with perpendicular magnetic anisotropy (PMA), SOT-induced deterministic magnetization switching typically necessitates an in-plane magnetic field to break the symmetry between up and down magnetization directions.[11,12] However, introducing an external field complicates the device architecture, which hinders high-density integration. Consequently, the pursuit of field-free deterministic magnetization switching remains a crucial area of research. Several solutions have been identified in related studies encompassing interlayer exchange coupling (IEC),[13,14] wedge structure,[15,16] exchange bias,[17,18] competing spin currents,[19] and z-direction spin currents,[20,21] amongst other approaches.[22–25] For field-free SOT-induced magnetization switching via IEC, two FM layers, one with in-plane magnetic anisotropy (IMA) and the other with PMA, are separated by a non-magnetic (NM) layer. The IMA layer provides an in-plane equivalent magnetic field for the PMA layer, thereby achieving field-free SOT switching. Moreover, the SOT-induced switching behavior can be modulated by pre-magnetizing the IMA layer.[14] On the other hand, the IMA layer can directly generate z-direction spin currents (σ_z) through anomalous SHE, which could contribute to field-free SOT-induced magnetization switching.[26]

Rare-earth-free Mn-based binary alloys, including $L1_0$-MnGa, $D0_{22}$-Mn_3Ga, and $L1_0$-MnAl, are promising for MRAM electrodes owing to their superior magnetic properties, such as significant PMA constants, high spin polarizations, high Curie temperature, and low magnetic damping constants.[27–32] Compared to other PMA Mn-based binary alloys, the $L1_0$-MnAl stands out being cost-effective, attributing to the abundant availability of Al, while maintaining substantial magnetic performance.[29,33–36] Furthermore, theoretical studies forecast the half metallicity at a Δ_1 band structure in $L1_0$-MnAl, with the tunnel magnetoresistance (TMR) ratio in $L1_0$-MnAl/MgO-based MTJ potentially exceeding 8000%, rendering it a suitable candidate for MTJ electrodes.[37] However, the bulk PMA of $L1_0$-MnAl, originating from magnetocrystalline anisotropy, necessitates a high-quality single crystalline structure. This requirement means the necessity for lattice-matching buffer lay-

*Corresponding author. Email: jhzhao@semi.ac.cn
© 2024 Chinese Physical Society and IOP Publishing Ltd

ers, which places rigorous demands on growth technology and stacking structure design and imposes constraints on applications of $L1_0$-MnAl. Current research on the SOT effect in Mn-based binary alloys mainly places traditional SCG, such as heavy metals (HMs), on the top of stacking structure, attributed to their ineffectiveness as buffers because of the lattice-mismatch issue.[38–42] However, in instances where $L1_0$-MnAl serves as the electrode in SOT-MTJ, employing a lattice-matching buffer as SCG is essential to ensure direct contact between $L1_0$-MnAl and the MgO barrier to guarantee the high thermal stability and TMR ratios of MTJ. Consequently, there is an urgent requirement for an appropriate material capable of serving both as a buffer and as an SCG layer for $L1_0$-MnAl alloy. Recent studies have demonstrated the excellent lattice-matching properties between paramagnetic B2-CoGa and Mn-based binary alloys.[43,44] In addition, B2-CoGa has been identified to exhibit considerable SHE arising from the $3d$–$4p$ orbital hybridization, enabling its function as an SCG layer.[45,46] These findings establish B2-CoGa as a unique material that meets the aforementioned requirements. Furthermore, as previously noted, for the realization of field-free SOT-induced magnetization switching via IEC, it is imperative that both the IMA layer and the SCG layer exhibit lattice matching with $L1_0$-MnAl. Research has shown that IMA Co-based full Heusler alloys Co_2MnX (X = Si, Ga, Al, Ge, Sn) can serve as a suitable buffer to enhance the PMA of the $L1_0$-MnAl layer.[32] These results provide beneficial references for applications of $L1_0$-MnAl in high-performance and field-free SOT-MRAM. However, studies pertaining to the SOT behavior in the $L1_0$-MnAl/B2-CoGa bilayer remain limited. Moreover, research on field-free SOT-induced magnetization switching behavior in the $L1_0$-MnAl alloy system is relatively scarce.

In this Letter, we systemically investigate the structural and magnetic properties of the $L1_0$-MnAl/B2-CoGa bilayer. An excellent PMA is obtained in the bilayer. Furthermore, we delve into the SOT-induced deterministic magnetization switching in the bilayer and have quantitatively evaluated the SOT efficiency. Moreover, we develop a multilayer stacking structure of $L1_0$-MnAl/B2-CoGa/Co_2MnGa, where the top $L1_0$-MnAl layer retains robust PMA and accomplishes field-free SOT-induced deterministic magnetization switching.

Sample preparation was carried out using a VG-V80 molecular-beam epitaxy (MBE) system with two interconnected growth chambers. The multilayers were grown on semi-insulating (SI) GaAs (001) substrates, employing top-bottom stacking structures of Al/$L1_0$-MnAl(2)/B2-CoGa(5)/GaAs and Al/$L1_0$-MnAl(2)/B2-CoGa(3)/Co_2MnGa(1.5)/GaAs (thicknesses in nanometers). Initially, the GaAs substrate was transferred into one growth chamber for deoxygenation and growth of a 200-nm-thick GaAs buffer layer, aiming to achieve a smooth interface. Subsequently, the substrate was transferred into another growth chamber for the growth of the metal multilayer. The CoGa layer was deposited, maintaining a nominal atomic ratio of 1 : 1 at 350 ℃. After growth, the substrate temperature was lowered to 300 ℃ to grow the MnAl layer. Finally, an Al layer was deposited on the top at room temperature to prevent oxidation. Characterization of the crystalline structure and magnetic properties was performed using x-ray diffraction (XRD) and superconductive quantum interface devices (SQUIDs). The XRD measurements were performed using the Cu $K_{\alpha 1}$ with a wavelength of 1.54056 Å and θ–2θ geometry. Subsequently, the samples were patterned into Hall devices through photolithography and ion beam etching (IBE) to perform the anomalous Hall effect (AHE), SOT-induced magnetization switching, and harmonic Hall voltage response (HHVR) measurements. Electrical characterization was conducted using the physical property measurements system (PPMS), combined with a Keithley 6221 current source, a 2182A nanovoltmeter, and a Stanford SR830 lock-in amplifier.

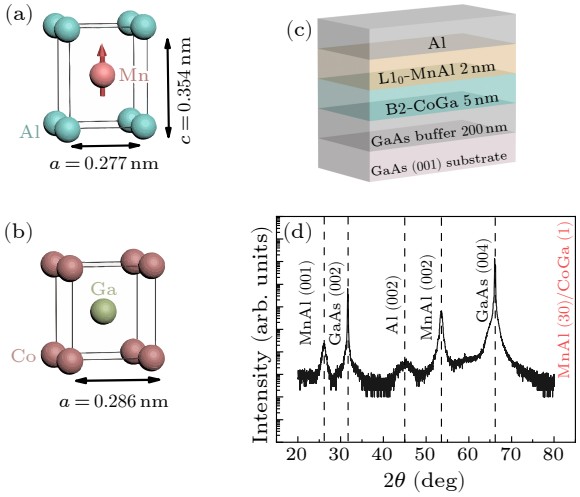

Fig. 1. [(a), (b)] Unit cells of tetragonal $L1_0$-MnAl and cubic B2-CoGa alloys. (c) Schematic stacking structure of the sample. (d) XRD patterns of $L1_0$-MnAl(30)/B2-CoGa(1) thin film.

Figures 1(a) and 1(b) illustrate the structure diagrams of tetragonal $L1_0$-MnAl and cubic B2-CoGa alloys.[47,48] Within the $L1_0$-MnAl structure, spins of adjacent Mn atoms align parallel to each other along the z axis, exhibiting ferromagnetism. The stacking structure of the samples is displayed in Fig. 1(c). For reference, we grew Al/MnAl(30)/CoGa(1)/GaAs structure for XRD characterization to investigate the structural properties of the MnAl layer. Figure 1(d) reveals distinct GaAs (002) and (004) substrate peaks, along with the (001) superlattice peak and (002) fundamental peak of MnAl, indicating the high (001) orientation. The pronounced intensity of the superlattice (001) peak suggests a high degree of chemical ordering in the $L1_0$-MnAl thin films, favorable for achieving superior PMA. In addition, the small values of full width at half maximum (FWHM) of the $L1_0$-MnAl peaks are indicative of a high-quality crystalline structure. The (001) and (002) peak positions have been determined to be 26.02° and 53.56°, respectively. According to Bragg's law, the lattice constant has been calculated to be 3.42 Å, marginally smaller than the bulk state value (3.54 Å) attributed to the strain effect.[30] These findings reveal that

$L1_0$-MnAl/B2-CoGa bilayers are capable of achieving excellent epitaxial growth on GaAs (001) substrates.

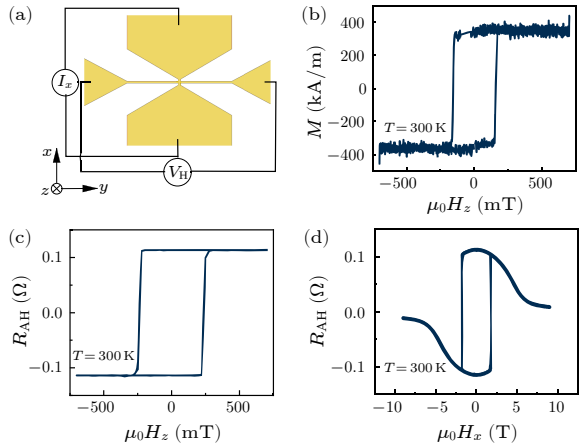

Fig. 2. (a) Hall device and measure schematic. (b) Hysteresis curve of the $L1_0$-MnAl(2)/B2-CoGa(5) structure. (c) Out-of-plane AHE curve of the $L1_0$-MnAl(2)/B2-CoGa(5) structure. (d) In-plane AHE curve of the $L1_0$-MnAl(2)/B2-CoGa(5) structure.

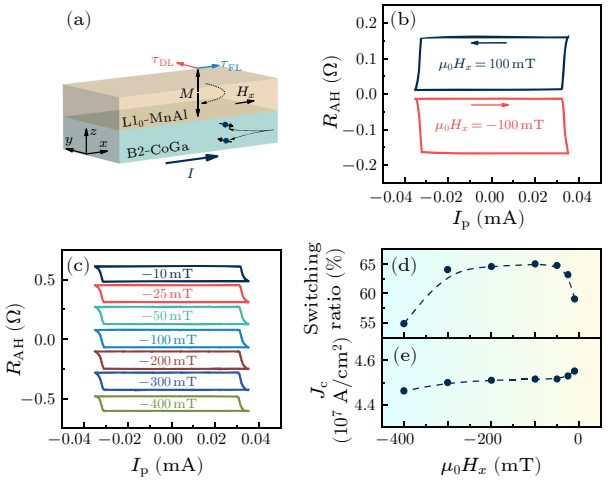

Fig. 3. (a) Schematic diagram of SOT-driven magnetization switching. (b) Deterministic magnetization switching of $L1_0$-MnAl(2)/B2-CoGa(5) under $\mu_0 H_x = \pm 100$ mT. (c) SOT-induced magnetization switching curves of the $L1_0$-MnAl(2)/B2-CoGa(5) structure for the different magnitude of $\mu_0 H_x$. (d) The variations of switching ratio and J_c with $\mu_0 H_x$.

Following the characterization of the crystalline structures, we further measured the magnetic properties of the $L1_0$-MnAl(2)/B2-CoGa(5) bilayer. The bilayer was patterned into the Hall device for electrical measurements, as illustrated in Fig. 2(a). The out-of-plane hysteresis loop and the AHE loop are shown in Figs. 2(b) and 2(c), respectively. The loops exhibit a high remanence ratio, indicating the good PMA of the bilayer, which is constant with the structural analysis. Moreover, the saturation magnetization (M_s) of the bilayer is determined to be 325.79 kA/m. To quantitatively assess the PMA, we characterize the effective perpendicular anisotropy field (H_k^{eff}) of the bilayer by measuring the in-plane AHE curves. As shown in Fig. 2(d), the R_{AH} value gradually decreases to zero as the in-plane external magnetic field increases, indicating that the perpendicular magnetization is progressively aligned parallel to the field. As a result, the value of $\mu_0 H_k^{\text{eff}}$ is determined to be 5.97 T. According to the formula $K_u = M_s^2/2\mu_0 + H_k^{\text{eff}} M_s/2$, the PMA constant ($K_u$) of the sample is determined to be 1.04×10^6 J/m^3. In our experiment, a higher PMA constant is achieved in 2-nm-thick $L1_0$-MnAl with B2-CoGa buffer, surpassing the values in the nanometer-thick $L1_0$-MnAl/B2-CoAl (8.5×10^5 J/m^3) and $L1_0$-MnGa/B2-CoGa (4×10^5 J/m^3) bilayer.[45,49] We have calculated the critical size d using the typical thermal stability condition $K_u d^3/k_B T \geq 60$, where k_B and T represent the Boltzmann constant and temperature, respectively. In this study, we have obtained $K_u = 1.04 \times 10^6$ J/m^3. At room temperature ($T = 300$ K), the value of d has been calculated to be 6.21 nm. The result represents that the $L1_0$-MnAl(2)/B2-CoGa(5) bilayer in our experiment is able to support the 6.21 nm diameter MTJ size to be capable of sustaining data integrity at room temperature for over ten years, thereby offering a substantial material foundation for the high-performance MRAM.

Based on the above results, we investigated the SOT-induced magnetization switching behaviors in the $L1_0$-MnAl(2)/B2-CoGa(5) bilayer. A series of pulsed currents with 50 μs duration were applied along the x-axis of the Hall device. Subsequently, a current of 0.1 mA was employed to measure the anomalous Hall resistance (R_{AH}) in the sample. An in-plane assistant magnetic field ($\mu_0 H_x$) was applied to achieve deterministic magnetization switching. As depicted in Fig. 3(b), under a $\mu_0 H_x = +100$ mT, the out-of-plane magnetization switches from down to up as the current sweeps from negative to positive, and it switches back when the current sweeps in the opposite direction. When the direction of $\mu_0 H_x$ is reversed, the switching orientation changes from counterclockwise to clockwise. The reversed switching direction observed under $\mu_0 H_x = \pm 100$ mT confirms the realization of SOT-induced deterministic magnetization switching. Additionally, the counterclockwise switching is exhibited under positive $\mu_0 H_x$, which is consistent with the previous finding that CoGa exhibits a positive effective SOT efficiency.[45] Subsequent investigations focus on the SOT-induced magnetization switching behavior of the samples under different magnitudes of $\mu_0 H_x$, as depicted in Fig. 3(c). Taking into account the shunt effect of the parallel circuit and using resistivity values of $\rho_{CoGa} = 175$ μΩ·cm and $\rho_{MnAl} = 165$ μΩ·cm, the critical switching current density (J_c) values of the sample, defined as the current density at which R_{AH} changes by half, have been meticulously calculated. Figures 3(d) and 3(e) illustrate the variation of the switching ratio and the J_c with different $\mu_0 H_x$ magnitudes. The value of J_c is determined to be 4.63×10^7 A/cm^2 under $\mu_0 H_x = 100$ mT, which is higher than the $L1_0$-MnGa/B2-CoGa bilayer (1.6×10^7 A/cm^2) due to the significantly larger K_u but is lower than the value in the Ta/$L1_0$-MnGa bilayer (8.5×10^7 A/cm^2).[39,45] Additionally, with the increase of $\mu_0 H_x$, the switching ratio initially increases to a peak value before beginning to decrease. The J_c decreases

with increasing $\mu_0 H_x$, yet the relationship is not strictly linear, suggesting that the switching process is governed by a magnetic domain correlation mechanism rather than the macro-spin model.[50] The situation is similar under positive $\mu_0 H_x$ changes and will not be reiterated here.

In the previous study of the $L1_0$-MnGa(2)/B2-CoGa(5) bilayer, the damping-like and field-like SOT efficiencies have been identified as $\xi_{DL} = 0.05$ and $\xi_{FL} = 0.27$, respectively. The damping-like SOT efficiency arises from the SHE induced by the $3d$–$4p$ orbital hybridization in CoGa alloy, while the substantial field-like SOT efficiency possibly originates from the special band matching at the $L1_0$-MnGa/B2-CoGa interface.[45] Based on previous results, we have quantitatively determined the ξ_{DL} and ξ_{FL} in the $L1_0$-MnAl(2)/B2-CoGa(5) system using the HHVR measurements. The schematic diagram of the HHVR measurements is shown in Fig. 4(a). In the $L1_0$-MnAl/B2-CoGa bilayer-based Hall device, applying an alternating current (AC) along the x- or y-axis induces the current-dependent SOT effective fields, including damping-like and field-like effective fields (H_{DL} and H_{FL}). These fields will periodically modulate the magnetization, which results in the generation of high-order harmonic Hall voltage signals. By measuring both the variation of the first and second-order harmonic Hall voltage signals in response to external magnetic field H_x and H_y, the H_{DL} and H_{FL} of the bilayer can be ascertained by the following equation:[41]

$$H_{DL(FL)} = -\frac{2\partial V_{2\omega}/\partial H_{x(y)}}{\partial^2 V_{1\omega}/\partial H_{x(y)}^2}. \quad (1)$$

Figure 4(b) displays the variation of the first harmonic Hall voltage signal $V_{1\omega}$ with H_x for both $\pm z$-direction magnetizations ($\pm M_z$). The variations of the $V_{1\omega}$ with both H_x and H_y are almost the same. Figures 4(c) and 4(d) illustrate the variations of the second harmonic Hall voltage signal $V_{2\omega}$ with H_x and H_y. The $V_{2\omega}$ signal demonstrates a strong linear correlation with the in-plane fields. Subsequently, we have calculated the damping-like and field-like SOT efficiency (ξ_{DL} and ξ_{FL}) of the bilayer using the following formula:

$$\xi_{DL(FL)} = \frac{2e}{\hbar}\frac{\mu_0 H_{DL(FL)} M_s t_{FM}}{J_0}, \quad (2)$$

where e is the electron charge, $\hbar$ is the reduced Planck constant, and t_{FM} is the thickness of the FM layer. We obtain $\xi_{DL} = 0.042 \pm 0.006$ and $\xi_{FL} = 0.059 \pm 0.002$, with the former being comparable to that in the $L1_0$-MnGa/B2-CoGa bilayer and the latter being significantly smaller. Previous studies on $L1_0$-MnGa/B2-CoGa and CoFeB/B2-CoGa revealed that the ξ_{FL} of the former (0.27) is significantly larger than that in the latter (0.03), and this difference was attributed to the sensitivity of ξ_{FL} to the interfacial band matching.[45] In our experiment, we infer that the reduced ξ_{FL} may also result from differences in interfacial band matching with $L1_0$-MnAl/B2-CoGa and $L1_0$-MnGa/B2-CoGa, which relies on further investigation. The realization of excellent PMA and SOT-induced deterministic magnetization switching makes the $L1_0$-MnAl/B2-CoGa bilayer an outstanding candidate for the electrode of SOT-MRAM.

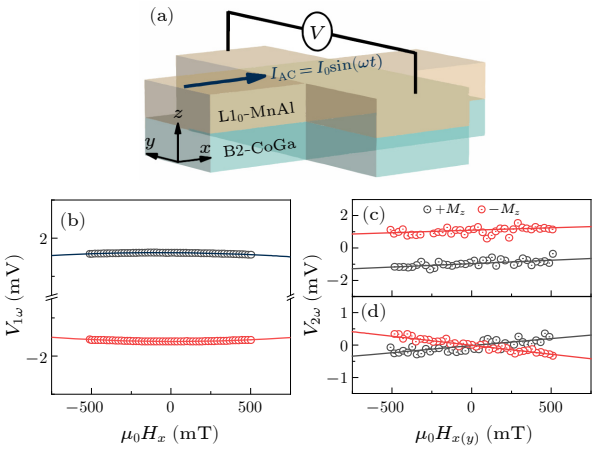

Fig. 4. (a) Schematic diagram of the HHVR measurement. (b) Variation of the first harmonic Hall voltage signal $V_{1\omega}$ with $\mu_0 H_x$. [(c), (d)] Variations of the second harmonic Hall voltage signal $V_{2\omega}$ with $\mu_0 H_x$ and $\mu_0 H_y$, respectively.

Table 1. The lattice constants of each layer and corresponding mismatch with $L1_0$-MnAl.

Layer	Space group	a (Å)	f (%)
GaAs	$F\bar{4}3m$	5.65[51]	2.0
B2-CoGa	$Pm\bar{3}m$	2.86[47]	3.1
Co_2MnGa	$Fm\bar{3}m$	5.77[51]	4.0
$L1_0$-MnAl	$P4/mmm$	2.77[48]	–

Furthermore, we designed an $L1_0$-MnAl-based multilayer employing IEC to realize field-free SOT-induced magnetization switching. The specific stacking structure comprises Al/$L1_0$-MnAl(2)/B2-CoGa(3)/Co_2MnGa(1.5) [Fig. 5(a)]. As shown in Table 1, the Co-based full Heusler alloy Co_2MnGa, belonging to the $Fm\bar{3}m$ space group with a lattice constant of 5.77 Å,[51] exhibits small lattice-mismatch with both GaAs, B2-CoGa, and $L1_0$-MnAl, which is capable of achieving epitaxial growth and providing IEC. The AHE curve, as shown in Fig. 5(b), displays a superposition of IMA and PMA. Notably, Co_2MnGa, as a Weyl semimetal, may also contribute spin currents with an effective SOT efficiency sign opposite to that of B2-CoGa.[52] To quantitatively estimate the SOT efficiency of the Co_2MnGa and CoGa layers in our study, we have utilized the following formula:[53]

$$J_s(t_{SCG})/J_s(t_{SCG} = \infty) = 1 - \mathrm{sech}(t_{SCG}/\lambda_s), \quad (3)$$

where t_{SCG} and λ_s represent the thickness and spin relaxation length of the SCG layer, respectively. By integrating the known SOT efficiencies of CoGa ($t_{CoGa} = 5$ nm, $\xi_{DL} = 0.042$) and Co_2MnGa ($t_{Co_2MnGa} = 10$ nm, $\xi_{DL} = -0.052$),[54] we have estimated the SOT efficiency of 1.5-nm-thick Co_2MnGa as -0.006, assuming λ_s to be 3 nm.[55] For the 3-nm-thick CoGa layer, the efficiency has been determined to be 0.023. Moreover, theoretical studies have demonstrated that σ_z can be generated in the IMA layer when the direction of the applied current is parallel to its magnetic moment.[26] In our experiments, σ_z may be generated in the Co_2MnGa layer and have an impact on field-free SOT-induced magnetization switching. Since σ_z

is expected to attenuate after passing through the CoGa layer with strong SOC, the actual effect of σ_z on $L1_0$-MnAl would be relatively minor. Therefore, we propose that the IEC primarily facilitates field-free SOT-induced magnetization switching in our structure while the σ_z plays a secondary role. As presented in Fig. 5(c), we have measured the SOT-induced magnetization switching behavior in the multilayer with an in-plane magnetic field changing from 50 to 0 mT. Initially, the sample was pre-magnetized (pre-mag.) with a 50 mT magnetic field applied along the $+x$ direction (H_x), and then H_x was gradually reduced to 0. During the process, Co_2MnGa remains magnetized in the $+x$ direction, providing an equivalent magnetic field along the $-x$ direction to $L1_0$-MnAl via the antiferromagnetic IEC. As shown in Fig. 5(c), the switching ratio decreases to 0 when the applied magnetic field reaches 1 mT, indicating that the H_x is compensated with the IEC field completely.[14,56] Under varying H_x, the σ_z generated in Co_2MnGa is consistently present and remains basically unchanged, as it is solely dependent on M and J of Co_2MnGa,[26] yet the σ_z is not strong enough to independently drive the magnetization switching. Consequently, we have determined the magnitude of the IEC field to be 1 mT.

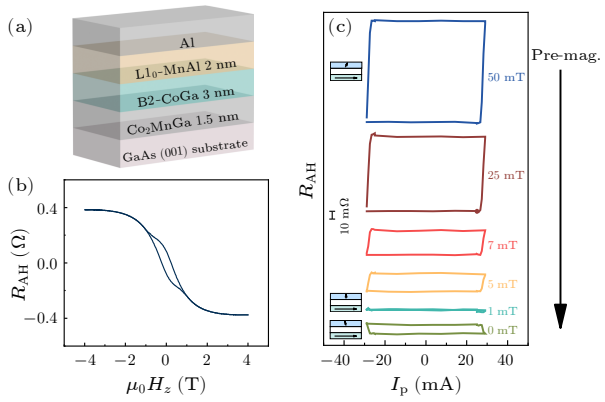

Fig. 5. [(a), (b)] Stacking structure and AHE curve of the multilayer, respectively. (c) SOT switching curves of the samples with in-plane magnetic field H_x changing from 50 to 0 mT.

Additionally, since the multilayer designed in our experiment incorporates CoGa and Co_2MnGa with SOT efficiencies of opposite signs, it is expected that their spin currents will be neutralized entirely through the adjustment of the relative thicknesses of the two layers in subsequent experiments, thereby enabling the study of the competing spin-current mechanism.[19] Increasing the resistivity difference between the IMA and NM layers by modulating their element compositions may facilitate the realization of spin-orbit procession at the interface.[57] In addition, although the SHE strength is weak due to the limited thickness of Co_2MnGa in our experiment, increasing its thickness is expected to realize the spin-Hall procession (SHP), as the σ_z generated by the SHP correlates with the SHE in the IMA layer.[58] Moreover, expanding our material system by substituting alloys with comparable lattice constants (e.g., CoGa-CoAl, Co_2MnGa-Co_2MnAl) could enable us to investigate additional phenomena. All these designs will advance the understanding of the above critical mechanisms in the $L1_0$-MnAl-based material system.

In summary, we have systematically investigated the structural and magnetic properties as well as the SOT-induced magnetization switching behaviors in the $L1_0$-MnAl/B2-CoGa bilayer. Furthermore, we have demonstrated an $L1_0$-MnAl-based stacking structure for field-free SOT-induced magnetization switching. By utilizing the B2-CoGa buffer layer, we have achieved large PMA constants K_u in 2-nm-thick $L1_0$-MnAl film, capable of supporting an MTJ size of 6.21 nm in diameter. Subsequently, SOT-induced deterministic magnetization switching in the $L1_0$-MnAl/B2-CoGa bilayer has been achieved, with an exploration into the properties of the switching behaviors under in-plane magnetic fields. The damping-like and field-like SOT efficiencies in the $L1_0$-MnAl/B2-CoGa bilayer have been ascertained through HHVR measurement, respectively. Furthermore, an $L1_0$-MnAl/B2-CoGa/Co_2MnGa multilayer structure has been designed for field-free SOT-induced magnetization switching. These findings offer an effective approach for developing high-performance SOT-MRAM based on $L1_0$-MnAl.

Acknowledgement. The work was supported by the Strategic Priority Research Program of the Chinese Academy of Sciences (Grant No. XDB44000000).

References

[1] Zhang H C, Ma X Y, Jiang C P, Yin J L, Lyu S Q, Lu S Y, Shang X T, Man B W, Zhang C, Li D D, Li S H, Chen W J, Liu H X, Wang G F, Cao K H, Wang Z H, and Zhao W S 2022 *J. Semicond.* **43** 102501
[2] Zhao Y, Yang J, Li B, Cheng X, Ye X, Wang X, Jia X, Wang Z, Zhang Y, and Zhao W 2023 *Sci. China Inf. Sci.* **66** 142401
[3] Apalkov D, Khvalkovskiy A, Watts S, Nikitin V, Tang X, Lottis D, Moon K, Luo X, Chen E, Ong A, Driskill-Smith A, and Krounbi M 2013 *ACM J. Emerg. Technol. Comput. Syst.* **9** 13
[4] Li Y, Kang W, Zhou K, Qiu K, and Zhao W 2023 *ACM Trans. Embed. Comput. Syst.* **22** 29
[5] Seo Y and Kwon K W 2023 *Electronics* **12** 4223
[6] de Orio R L, Makarov A, Selberherr S, Goes W, Ender J, Fiorentini S, and Sverdlov V 2020 *Solid State Electron.* **168** 107730
[7] Liu L, Pai C F, Li Y, Tseng H W, Ralph D C, and Buhrman R A 2012 *Science* **336** 555
[8] Zhang S 2000 *Phys. Rev. Lett.* **85** 393
[9] Hirsch J E 1999 *Phys. Rev. Lett.* **83** 1834
[10] Edelstein V M 1990 *Solid State Commun.* **73** 233
[11] Liu L, Lee O J, Gudmundsen T J, Ralph D C, and Buhrman R A 2012 *Phys. Rev. Lett.* **109** 096602
[12] Lee O J, Liu L Q, Pai C F, Li Y, Tseng H W, Gowtham P G, Park J P, Ralph D C, and Buhrman R A 2014 *Phys. Rev. B* **89** 024418
[13] Lau Y C, Betto D, Rode K, Coey J M D, and Stamenov P 2016 *Nat. Nanotechnol.* **11** 758
[14] Sheng Y, Edmonds K W, Ma X, Zheng H, and Wang K 2018 *Adv. Electron. Mater.* **4** 1800224
[15] Chen T Y, Chan H I, Liao W B, and Pai C F 2018 *Phys. Rev. Appl.* **10** 044038
[16] Li Y, Zhao X, Liu W, Wu J, Liu L, Song Y, Ma J, and Zhang Z 2023 *Appl. Phys. Lett.* **123** 032403
[17] Fukami S, Zhang C, DuttaGupta S, Kurenkov A, and Ohno H 2016 *Nat. Mater.* **15** 535

[18] Choi W C, Yoon S, Kim H J, Ha J H, Park K J, Baek E, Kim D R, Shin Y, You C Y, Kim J W, and Hong J I 2023 *APL Mater.* **11** 121115
[19] Ma Q, Li Y, Gopman D B, Kabanov Y P, Shull R D, and Chien C L 2018 *Phys. Rev. Lett.* **120** 117703
[20] Hamamoto K, Ezawa M, Kim K W, Morimoto T, and Nagaosa N 2017 *Phys. Rev. B* **95** 224430
[21] Han R K, Zhao X P, Qin H R, Sun H L, Wang H L, Wei D H, and Zhao J H 2023 *Phys. Rev. B* **107** 134422
[22] Zhang K, Chen L, Zhang Y, Hong B, He Y, Lin K, Zhang Z, Zheng Z, Feng X, Zhang Y, Otani Y, and Zhao W 2022 *Appl. Phys. Rev.* **9** 011407
[23] Wang M X, Cai W L, Zhu D Q, Wang Z H, Kan J, Zhao Z Y, Cao K H, Wang Z L, Zhang Y G, Zhang T R, Park C, Wang J P, Fert A, and Zhao W S 2018 *Nat. Electron.* **1** 582
[24] You Y, Bai H, Feng X, Fan X, Han L, Zhou X, Zhou Y, Zhang R, Chen T, Pan F, and Song C 2021 *Nat. Commun.* **12** 6524
[25] Kondou K, Chen H, Tomita T, Ikhlas M, Higo T, MacDonald A H, Nakatsuji S, and Otani Y 2021 *Nat. Commun.* **12** 6491
[26] Wang X R 2021 *Commun. Phys.* **4** 55
[27] Zhu L J, Nie S H, Meng K K, Pan D, Zhao J H, and Zheng H Z 2012 *Adv. Mater.* **24** 4547
[28] El-Gendy A A and Hadjipanayis G 2015 *J. Phys. D* **48** 125001
[29] Park J H, Hong Y K, Bae S, Lee J J, Jalli J, Abo G S, Neveu N, Kim S G, Choi C J, and Lee J G 2010 *J. Appl. Phys.* **107** 09A731
[30] Nie S H, Zhu L J, Lu J, Pan D, Wang H L, Yu X Z, Xiao J X, and Zhao J H 2013 *Appl. Phys. Lett.* **102** 152405
[31] Nie S H, Zhu L J, Pan D, Lu J, and Zhao J H 2013 *Acta Phys. Sin.* **62** 178103 (in Chinese)
[32] Mao S W, Lu J, Yang L, Ruan X Z, Wang H L, Wei D H, Xu Y B, and Zhao J H 2020 *Chin. Phys. Lett.* **37** 058501
[33] Sakuma A 1994 *J. Phys. Soc. Jpn.* **63** 1422
[34] Mizukami S, Wu F, Sakuma A, Walowski J, Watanabe D, Kubota T, Zhang X, Naganuma H, Oogane M, Ando Y, and Miyazaki T 2011 *Phys. Rev. Lett.* **106** 117201
[35] Sakuma A 1998 *J. Magn. Magn. Mater.* **187** 105
[36] Yang Z X, Li J, Wang D s, Zhang K M, and Xie X D 1998 *J. Magn. Magn. Mater.* **182** 369
[37] Zhang X, Tao L L, Zhang J, Liang S H, Jiang L, and Han X F 2017 *Appl. Phys. Lett.* **110** 252403
[38] Ranjbar R, Suzuki K Z, Sasaki Y, Bainsla L, and Mizukami S 2016 *Jpn. J. Appl. Phys.* **55** 120302
[39] Meng K, Miao J, Xu X, Wu Y, Xiao J, Zhao J, and Jiang Y 2016 *Sci. Rep.* **6** 38375
[40] Zhao X P, Sun H L, Tong S C, Han R K, Qin H R, and Zhao J H 2023 *Appl. Phys. Lett.* **123** 042407
[41] Zhao X P, Lu J, Mao S W, Yu Z F, Wei D H, and Zhao J H 2019 *Appl. Phys. Lett.* **115** 142405
[42] Meng K K, Miao J, Xu X G, Wu Y, Zhao X P, Zhao J H, and Jiang Y 2017 *Appl. Phys. Lett.* **110** 142401
[43] Oshima D, Kato T, and Iwata S 2020 *AIP Adv.* **10** 025012
[44] Suzuki K Z, Ranjbar R, Sugihara A, Miyazaki T, and Mizukami S 2016 *Jpn. J. Appl. Phys.* **55** 010305
[45] Lau Y C, Lee H, Qu G X, Nakamura K, and Hayashi M 2019 *Phys. Rev. B* **99** 064410
[46] Takikawa M, Suzuki K Z, Ranjbar R, and Mizukami S 2017 *Appl. Phys. Express* **10** 073004
[47] Mizukami S, Suzuki K Z, and Miura Y 2019 *Appl. Phys. Express* **12** 043003
[48] Sands T, Harbison J P, Leadbeater M L, Allen S J, Hull G W, Ramesh R, and Keramidas V G 1990 *Appl. Phys. Lett.* **57** 2609
[49] Takeuchi Y, Okuda R, Igarashi J, Jinnai B, Saino T, Ikeda S, Fukami S, and Ohno H 2022 *Appl. Phys. Lett.* **120** 052404
[50] Deng Y, Yang M, Ji Y, and Wang K 2020 *J. Magn. Magn. Mater.* **496** 165920
[51] Damsgaard C D, Hickey M C, Holmes S N, Feidenhans'l R, Mariager S O, Jacobsen C S, and Hansen J B 2009 *J. Appl. Phys.* **105** 124502
[52] Tang K, Wen Z, Lau Y C, Sukegawa H, Seki T, and Mitani S 2021 *Appl. Phys. Lett.* **118** 062402
[53] Bass J and Pratt W P 2007 *J. Phys.: Condens. Matter.* **19** 183201
[54] Safi T S, Chou C T, Hou J T, Han J, and Liu L 2022 *Appl. Phys. Lett.* **121** 092404
[55] Aoki M, Yin Y, Granville S, Zhang Y, Medhekar N V, Leiva L, Ohshima R, Ando Y, and Shiraishi M 2023 *Nano Lett.* **23** 6951
[56] Zhao X, Sun H, Han R, Qin H, Wen L, Wang H, Wei D, and Zhao J 2024 *APL Mater.* **12** 041103
[57] Baek S C, Amin V P, Oh Y W, Go G, Lee S J, Lee G H, Kim K J, Stiles M D, Park B G, and Lee K J 2018 *Nat. Mater.* **17** 509
[58] Hibino Y, Taniguchi T, Yakushiji K, Fukushima A, Kubota H, and Yuasa S 2021 *Nat. Commun.* **12** 6254